PLOS ONE

RESEARCH ARTICLE

Differential requirement of NPHP1 for compartmentalized protein localization during photoreceptor outer segment development and maintenance

Poppy Datta[1,2☯], **J. Thomas Cribbs**[1,2☯], **Seongjin Seo**[1,2*]

1 Department of Ophthalmology and Visual Sciences, The University of Iowa Carver College of Medicine, Iowa City, IA, United States of America, **2** Institute for Vision Research, The University of Iowa, Iowa City, IA, United States of America

☯ These authors contributed equally to this work.
* seongjin-seo@uiowa.edu

Citation: Datta P, Cribbs JT, Seo S (2021) Differential requirement of NPHP1 for compartmentalized protein localization during photoreceptor outer segment development and maintenance. PLoS ONE 16(5): e0246358. https://doi.org/10.1371/journal.pone.0246358

Editor: Hemant Khanna, University of Massachusetts Medical School, UNITED STATES

Received: December 17, 2020

Accepted: April 20, 2021

Published: May 7, 2021

Data Availability Statement: All relevant data are within the manuscript and its Supporting Information files.

Funding: This work was supported by National Institutes of Health grants R01-EY022616 and R21-EY027431 (to S.S.), National Institutes of Health Center Support grant P30-EY025580 (to the University of Iowa), and Research to Prevent Blindness Unrestricted Grant (to the Department of Ophthalmology and Visual Sciences, University of Iowa). The funders had no role in study design,

Abstract

Nephrocystin (NPHP1) is a ciliary transition zone protein and its ablation causes nephronophthisis (NPHP) with partially penetrant retinal dystrophy. However, the precise requirements of NPHP1 in photoreceptors are not well understood. Here, we characterize retinal degeneration in a mouse model of NPHP1 and show that NPHP1 is required to prevent infiltration of inner segment plasma membrane proteins into the outer segment during the photoreceptor maturation. We demonstrate that *Nphp1* gene-trap mutant mice, which were previously described as null, are likely hypomorphs due to the production of a small quantity of functional mRNAs derived from nonsense-associated altered splicing and skipping of two exons including the one harboring the gene-trap. In homozygous mutant animals, inner segment plasma membrane proteins such as syntaxin-3 (STX3), synaptosomal-associated protein 25 (SNAP25), and interphotoreceptor matrix proteoglycan 2 (IMPG2) accumulate in the outer segment when outer segments are actively elongating. This phenotype, however, is spontaneously ameliorated after the outer segment elongation is completed. Consistent with this, some photoreceptor cell loss (~30%) occurs during the photoreceptor maturation period but it stops afterward. We further show that *Nphp1* genetically interacts with *Cep290*, another NPHP gene, and that a reduction of *Cep290* gene dose results in retinal degeneration that continues until adulthood in *Nphp1* mutant mice. These findings demonstrate that NPHP1 is required for the confinement of inner segment plasma membrane proteins during the outer segment development, but its requirement diminishes as photoreceptors mature. Our study also suggests that additional mutations in other NPHP genes may influence the penetrance of retinopathy in human NPHP1 patients.

data collection and analysis, decision to publish, or preparation of the manuscript.

Competing interests: The authors have declared that no competing interests exist.

Introduction

Photoreceptor cells in the retina are structurally and functionally compartmentalized. Proteins that transduce light into chemical and electrical signals are confined to an apical compartment called the outer segment (OS). This structure is an elaborate modification of primary cilia, which exist in most cells in vertebrates (see [1, 2] for a comprehensive review). In contrast, energy production and protein/lipid synthesis occur in another compartment, the inner segment (IS). Constituents of the OS are synthesized in the IS and transported to the OS through a narrow channel, the connecting cilium. The connecting cilium is equivalent to the transition zone in primary cilia and plays critical roles in regulating protein trafficking and confinement between the IS and the OS [3].

Nephrocystin (also known as NPHP1) is a protein that localizes to the connecting cilium in photoreceptors and the transition zone in primary cilia [4–9]. At the transition zone, NPHP1 is a part of a multi-protein complex that functions as a gate to control protein trafficking in and out of the ciliary compartment [8–13]. Ablation of individual components in this complex causes a group of related diseases, including nephronophthisis (NPHP), Joubert syndrome (JBTS), and Meckel-Gruber syndrome (MKS) [14, 15]. Retinal anomalies are common in patients with these diseases. While *NPHP1* is primarily associated with NPHP [16–19], a subset (6–10%) of NPHP1 patients exhibits retinal dystrophy as an extra-renal manifestation [19, 20]. This suggests a role of NPHP1 in photoreceptors. However, its precise functions in photoreceptors and the molecular/genetic basis of the incomplete penetrance are not well understood.

Two NPHP1 mouse models have been described thus far. In one model ($Nphp1^{del20}$), the last exon (exon 20) was deleted, and homozygous mutant animals displayed severe retinal degeneration with OS morphogenesis defects [5, 21]. $Nphp1^{del20/del20}$ animals also exhibited male infertility due to a defect in spermatogenesis [21]. The second model ($Nphp1^{neo}$; hereafter referred to as $Nphp1^{gt}$) was generated by an insertion of a gene-trap (a *PGK-neo-pA* cassette) into exon 4 (**S1 Fig**) [22]. This mutation was expected to generate a null allele because it disrupted the reading frame of *Nphp1*. However, retinal degeneration in this model was significantly milder than that of $Nphp1^{del20}$ mice: a slight reduction of the photoreceptor cell layer was observed at postnatal (P) day P21 and 2 months of age, and rhodopsin (RHO) trafficking was only marginally affected. Retinal phenotypes in older animals were not reported. The basis of this phenotypic difference in severity between these two mouse models is unknown, but disparities in the genetic background were suggested as a potential contributing factor [22]. Currently, only the $Nphp1^{gt}$ model is available to the research community and has been used in several studies to investigate genetic interactions with other ciliopathy genes [9, 23, 24].

We previously proposed that the OS acts as a sink for membrane proteins because of its large size, high membrane content, and continuous renewal [3]. This also suggests that accumulation of IS membrane proteins in the OS would be a common pathomechanism of retinal degenerations associated with ciliary gate defects. Indeed, IS plasma membrane-associated proteins including syntaxin-3 (STX3), syntaxin-binding protein 1 (STXBP1), synaptosomal-associated protein 25 (SNAP25), and interphotoreceptor matrix proteoglycan 2 (IMPG2) rapidly accumulate in the OS when the function of CEP290, another component of the ciliary gate complex, is compromised [25]. Notably, inactivating mutations in *CEP290* cause Leber congenital amaurosis (LCA), an early-onset severe retinal degeneration, in humans [26–29]. In this work, we sought to determine the requirement of NPHP1 for protein confinement in photoreceptors and test whether the aforementioned pathomechanism underlies retinal degeneration in *NPHP1*-associated retinopathies.

Materials and methods

Mouse and genotyping

Nphp1^{gt} and *Cep290*^{fl} mice were previously described [22, 30] and obtained from the Jackson laboratory (*Nphp1*^{tm1Jgg}/J, #013169; *Cep290*^{tm1Jgg}/J, #013701). *iCre75* mice were a generous gift from Dr. Ching-Kang Chen [31]. The lack of *rd1* mutation (in *Pde6b*) was confirmed by PCR using primers described in [25]. The *rd8* mutation (in *Crb1*) was eliminated by breeding. All animals used in this study were *Pde6b*$^{+/+}$;*Crb1*$^{+/+}$. For genotyping, mouse tail snips were collected at the time of weaning (P19-P24) or after euthanasia. Tail DNAs were extracted by Proteinase K digestion (Sigma-Aldrich; RPROTK-RO) in Tail Lysis Buffer (10 mM Tris pH 8.0, 100 mM NaCl, 10 mM EDTA, 1% SDS, 0.3 mg/ml Proteinase K) followed by ethanol precipitation. Genotyping was conducted by PCR using GoTaq G2 Flexi DNA polymerase (Promega) and primers listed in **Table 1**. PCR protocols are available upon request. All animals were maintained in 12-hour light/dark cycles and fed *ad libitum* standard mouse chow. All animal procedures were approved by the Institutional Animal Care and Use Committee (IACUC) of the University of Iowa (Protocol#: 8011301) and conducted following the recommendations in the Guide for the Care and Use of Laboratory Animals of the National Institutes of Health.

Plasmids and antibodies

A full-length mouse *Nphp1* coding sequence (BC118953) was obtained from Transomic Technologies. FLAG-tagged NPHP1 expression vectors (pCS2FLAG-NPHP1 (full-length), pCS2FLAG-NPHP1 Δ(49–110), and pCS2FLAG-NPHP1 aa242-685) were generated by inserting PCR-amplified DNA fragments into the EcoRI-XhoI sites of the pCS2FLAG plasmid, which was produced by replacing the 6x Myc tag with a 3x FLAG tag in the pCS2+MT vector [32], using a GenBuilder cloning kit (GenScript). pCS2HA-NPHP1 and pCS2HA-NPHP1 Δ (49–110) were generated by inserting the same PCR fragments into the pCS2HA vector [25]. Expression vectors pEGFP-NPHP2 and pEGFP-NPHP5 were generous gifts from Drs. Val C. Sheffield and William Y. Tsang, respectively. All constructs were sequence-verified by Sanger

Table 1. Primers used in this study.

Purpose	Primer	Sequence	PCR product
Nphp1	F1-mNPHP1-RT	GTGCTCTGGAACCGAGTAAA	wt: 991 bp
RT-PCR	R1-mNPHP1-RT	TGTCTGCTGAGAACCTGTATG	gt: 805 bp
Nphp1	F-mNPHP1-WT	ACATTTATGGAATCTGGGGTAG	wt: 289 bp
genotyping	R-mNPHP1-comm	CCCCGCTAGAGTATGGTCTG	gt: ~400 bp
	F-mNPHP1-GT	CGCCTTCTATCGCCTTCTTG	
iCre75	F-iCre75	TCAGTGCCTGGAGTTGCGCTGTGG	wt: none
genotyping	R-iCre75	CTTAAAGGCCAGGGCCTGCTTGGC	Tg: 650 bp
Cep290^{fl}	R2-Cep290-wt	GAATGCCCGCTACAGAAGAA	wt: 535 bp
genotyping	F2-Cep290-comm	CAGCAGCTGAGGAACGTATAA	fl: 426 bp
	R2-Cep290-mut	CTACCGGTGGATGTGGAATG	
Crb1 / rd8	F3-mCrb1-wt	GAAGACAGCTACAGTTCTTCTC	wt: 388 bp
genotyping	R3-mCrb1-comm	CACCTATGGACGGACATTTA	rd8: 388 bp
	F3-mCrb1-rd8	GAAGACAGCTACAGTTCTTCTG	(separate reactions)
Nphp1	F-mNPHP1-qRT	TGGTGAGAGAGGAGAGTTAAG	105 bp
qRT-PCR	R-mNPHP1-qRT	CCGCCATTCAAGAAGAGTT	
Rpl19	F-mRPL19-60	GCAAGCCTGTGACTGTCCATT	106 bp
qRT-PCR	R-mRPL19-60	GCATTGGCAGTACCCTTCCTC	

https://doi.org/10.1371/journal.pone.0246358.t001

Table 2. Antibodies used in this study.

Antibody	Source	Cat#	Verification
mouse anti-β-actin monoclonal (clone: AC-15)	Sigma-Aldrich	A1978	[33, 34]
mouse anti-ABCA4 monoclonal (clone: 3F4)	EMD Millipore	MABN2439	[35, 36]
Rabbit anti-ARL13B polyclonal	ProteinTech	17711-1-AP	[37]
mouse anti-FLAG monoclonal (clone: M2)	Sigma-Aldrich	F1804	not applicable
rabbit anti-GFP monoclonal	Invitrogen	G10362	not applicable
rabbit anti-GNAT2 polyclonal	Abcam	ab97501	[38]
rat anti-HA monoclonal (clone: 3F10)	Sigma/Roche	12158167001	not applicable
rabbit anti-IMPG2 polyclonal	Sigma-Aldrich	HPA008779	[25, 39]
rabbit anti-NPHP1 polyclonal	Abclonal	A6674	this study
rabbit anti-OPN1MW polyclonal	EMD Millipore	AB5405	[40, 41]
rabbit anti-PDE6B polyclonal	ProteinTech	22063-1-AP	[38]
rabbit anti-PRPH2 polyclonal	ProteinTech	18109-1-AP	[38]
mouse anti-RHO monoclonal (clone: 1D4)	EMD Millipore	MAB5356	[42]
rabbit anti-ROM1 polyclonal	ProteinTech	21984-1-AP	[38]
rabbit anti-RPGRIP1L polyclonal	ProteinTech	55160-1-AP	this study; S2 Fig
mouse anti-SNAP25 monoclonal (clone: SMI81)	Abcam	ab24737	[38]
mouse anti-STX3 monoclonal (clone: 1–146)	EMD Millipore	MAB2258	[34]
rabbit anti-STXBP1 polyclonal	ProteinTech	11459-1-AP	[38]
rabbit anti-γ-tubulin polyclonal	Sigma	T3559	[43]

https://doi.org/10.1371/journal.pone.0246358.t002

sequencing. Antibodies used for immunoblotting and immunohistochemistry are described in Table 2.

Immunoblotting

To extract proteins from mouse testes, animals were euthanized by CO_2 asphyxiation followed by cervical dislocation, and testicles were removed. Collected testicles were homogenized with Polytron PT 1200E (Kinematica) in an ice-cold lysis buffer (50 mM HEPES pH7.0, 150 mM NaCl, 2 mM $MgCl_2$, 2 mM EGTA, 1% Triton X-100) supplemented with Protease Inhibitor Cocktail (Bimake). Homogenates were clarified by centrifugation at 20,000x g for 15 min at 4˚C and supernatants were collected. Protein concentrations were measured using a DC Protein Assay kit (Bio-Rad) with BSA protein standards and AccuSkan GO spectrophotometer (Fisher Scientific). Fifty μg of proteins were mixed with NuPAGE LDS Sample Buffer (Invitrogen) and Reducing Agent (Invitrogen) and loaded on a 4–12% (wt/vol) NuPAGE Bis-Tris gel (Invitrogen). After electrophoresis, proteins were transferred to a 0.45-μm nitrocellulose membrane (Bio-Rad). Immunoblotting was performed following standard protocols, and primary antibodies used are listed in Table 2. Proteins were detected with horseradish peroxidase (HRP)-linked anti-mouse IgG and anti-rabbit IgG secondary antibodies (Cell Signaling; Cat# 7076 and 7074) and SuperSignal West Dura Extended Duration Substrate (Thermo Scientific). Images were taken with a ChemiDoc system (Bio-Rad).

Immunohistochemistry

Mouse eyes were collected, fixed, and embedded in Neg-50 Frozen Section Medium (Richard-Allan Scientific) as previously described [25]. Frozen eyecups were mounted on a cryostat chuck in an orientation that sections became perpendicular to the retinal plane at the central retina. Eight-μm thick, serial sections were collected from the middle 1/3 of eyecups and used for immunohistochemistry. Immunostaining, imaging, and quantification procedures were

previously described elsewhere [25]. To assess the photoreceptor cell loss, 3 serial sections that contained the central retina were selected and the number of rows of photoreceptor cell nuclei was counted near the center of the retina (300–600 μm from the optic nerve head; 2 locations/section). OS lengths were measured in the same sections. For statistical analysis, unpaired two-tailed *t* test or one-way ANOVA followed by Tukey's multiple comparison test was performed using GraphPad Prism software (version 9.1.0). *P* values smaller than 0.01 were regarded as statistically significant.

mIMCD-3 cells were obtained from ATCC (#CRL-2123) and cultured in DMEM:F12 Medium (Invitrogen) supplemented with 10% fetal bovine serum (Sigma), 100 units/mL of penicillin, and 100 μg/mL of streptomycin (Invitrogen). HA-tagged NPHP1 expression vectors were transfected to mIMCD-3 cells using FuGENE HD (Promega) following the manufacturer's instruction. Immunostaining and imaging procedures are described in [37].

Electroretinogram (ERG)

Mice were dark-adapted overnight before ERG recording. Under dim red light illumination, mice were anesthetized by intraperitoneal injection of a ketamine/xylazine mixture (87.5 mg/kg and 12.5 mg/kg, respectively), and pupils were dilated with 1% tropicamide ophthalmic solution (Akorn) for 2–3 minutes. Mice were placed on a Celeris D430 rodent ERG testing system (Diagnosys) with its heater on to maintain animals' body temperature. After applying GenTeal Tears Lubricant Eye Gel (Alcon), light-guide electrodes were positioned on both eyes. For dim light scotopic ERG, responses were measured with 15 flashes of 0.01 cd·sec/m^2 stimulating light (color temperature: 6500K). Dark-adapted Standard Combined Response (SCR) was measured with 15 flashes of 3.0 cd·sec/m^2 stimulating light (color temperature: 6500K). For photopic ERG, mice were light-adapted with rod-saturating white background light (9.0 cd·sec/m^2) for 10 minutes, and responses were measured with 15 flashes of 3.0 cd·sec/m^2 white light (6500K) in the presence of the background light. After recording, animals were allowed to recover on a heating pad.

RNA extraction, Reverse Transcription (RT)-PCR, and quantitative PCR

Tissue collection and RNA extraction procedures were described previously [25]. *Nphp1* cDNA fragments spanning exons 2 to 11 were PCR-amplified using Universe High-Fidelity Hot Start DNA polymerase (Bimake) and two primers (F1-mNPHP1-RT and R1-mNPHP1-RT) listed in **Table 1**. PCR products were directly sequenced by Sanger sequencing using the F1-mNPHP1-RT primer. Band intensities were measured using the Image Lab software (Bio-Rad). Quantitative real-time PCR was performed as previously described [34] using primers listed in **Table 1**.

Immunoprecipitation

HEK 293T/17 cells were obtained from ATCC (#CRL-11268) and cultured in Dulbecco's Modified Eagle's Medium (DMEM; Invitrogen) supplemented with 10% fetal bovine serum (Sigma), 100 units/mL of penicillin, and 100 μg/mL of streptomycin (Invitrogen). GFP-NPHP2 and GFP-NPHP5 expression vectors were transiently transfected to 293T/17 cells together with pCS2FLAG empty vectors (as a control) or pCS2FLAG-NPHP1 variants using FuGENE HD (Promega), following the manufacturer's instruction. Protein extracts were prepared and subjected to immunoprecipitation with anti-FLAG M2 magnetic beads (Sigma) as previously described [25]. SDS-PAGE and immunoblotting were performed as described above.

Results

Mislocalization of inner segment plasma membrane-associated proteins in *Nphp1*$^{gt/gt}$ retinas

To test the requirement of NPHP1 for compartmentalized protein localization in photoreceptors, we probed the localization of various IS and OS resident proteins in *Nphp1*$^{gt/gt}$ mouse retinas. Our prior study showed that IS plasma membrane proteins STX3, STXBP1, SNAP25, and IMPG2 were the most susceptible to mislocalization in CEP290-deficient photoreceptors [25]. Therefore, we focused our efforts on these proteins. In normal photoreceptors, these proteins were strictly restricted to the IS (hereafter our use of the term IS encompasses all parts of photoreceptors except the OS) (Fig 1). In 18-day old *Nphp1*$^{gt/gt}$ mutants, however, all of these proteins showed significant mislocalization to the OS (Fig 1A–1D; see Fig 1E for quantification). STXBP1 showed the most severe mislocalization with approximately 1/3 of proteins mislocalized to the OS. Consistent with the previous finding [22], mislocalization of RHO to the IS was relatively mild in *Nphp1*$^{gt/gt}$ mutants and no mislocalization was detected with other OS resident proteins examined (PRPH2, ROM1, ABCA4, and PDE6B) (Fig 1 **and** S3 Fig). In addition to protein mislocalization, OSs were approximately 40% shorter in *Nphp1*$^{gt/gt}$ mutants compared with control animals (mean ± SD: 14.00 ± 1.53 μm in *Nphp1*$^{gt/gt}$ vs. 23.47 ± 1.28 μm in *Nphp1*$^{+/gt}$; n = 4; $p < 0.01$) (Fig 1F).

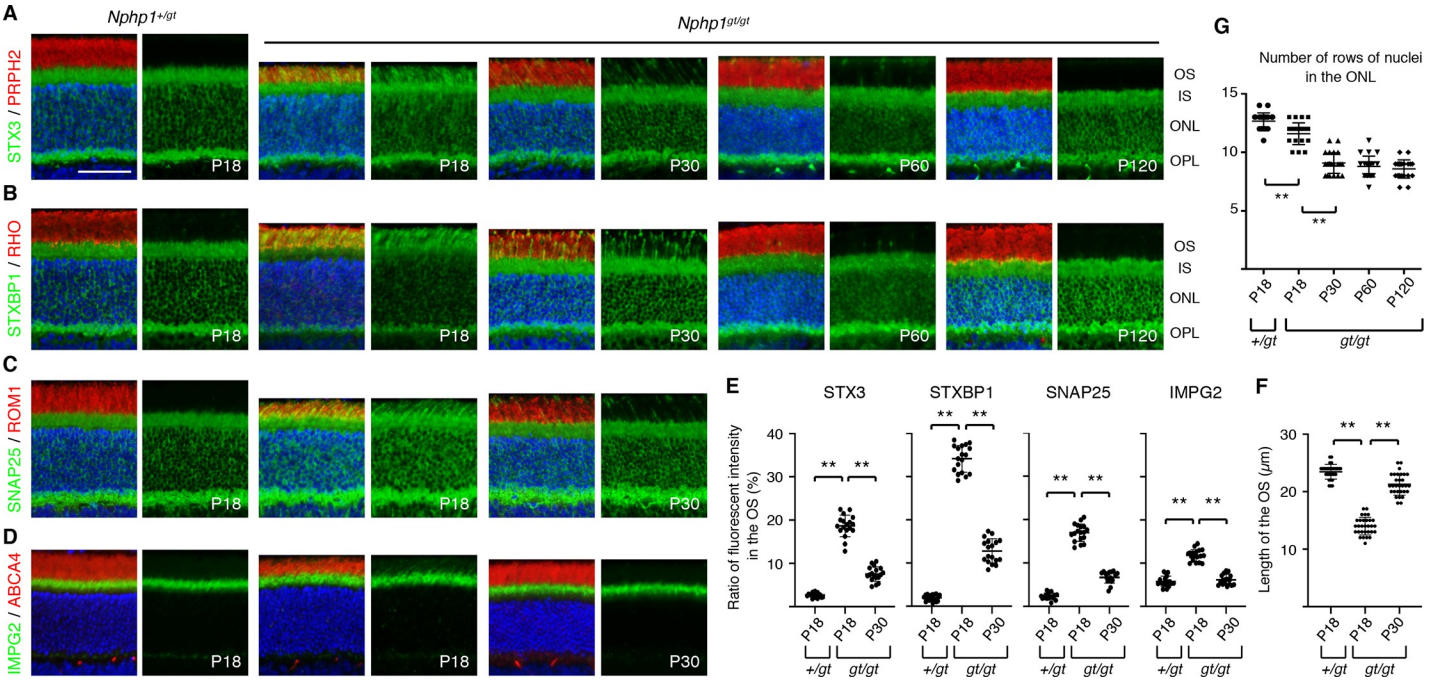

Fig 1. Protein confinement defects and photoreceptor cell loss in *Nphp1*$^{gt/gt}$ mice. (A-D) Transient mislocalization of STX3 (A), STXBP1 (B), SNAP25 (C), and IMPG2 (D) in *Nphp1*$^{gt/gt}$ retinas. Retinal sections from *Nphp1*$^{+/gt}$ and *Nphp1*$^{gt/gt}$ mice were stained with STX3, STXBP1, SNAP25, and IMPG2 antibodies (green). PRPH2, RHO, ROM1, and ABCA4 (red) were labeled as a marker of the OS. Merged images are shown on the left. DAPI (blue) was used to counterstain the nuclei. Scale bar denotes 50 μm. IS: inner segment, ONL: outer nuclear layer, OPL: outer plexiform layer. OS: outer segment. (E) Quantification of IS membrane protein mislocalization to the OS. Depicted are the ratios of integrated fluorescence intensities in the OS relative to the photoreceptor cell layer. Means ± standard deviations (SD; error bars) are marked by horizontal lines (n = 3 mice; 2 sections/mouse and 3 areas/section). (F) Transient shortening of the OS in *Nphp1*$^{gt/gt}$ retinas. The length of the OS was measured in *Nphp1*$^{+/gt}$ and *Nphp1*$^{gt/gt}$ mice at the central retina, and mean ± SD is depicted (n = 4 mice; 3 sections/mouse; 2–3 locations/section). (G) Photoreceptor cell loss in *Nphp1*$^{gt/gt}$ retinas. The number of rows of photoreceptor cell nuclei was counted in *Nphp1*$^{+/gt}$ and *Nphp1*$^{gt/gt}$ mice at the central retina (n = 4 mice; 3 sections/mouse; 2 locations/section). Asterisks indicate statistical significance (one-way ANOVA followed by Tukey's multiple comparison test; $p < 0.01$).

https://doi.org/10.1371/journal.pone.0246358.g001

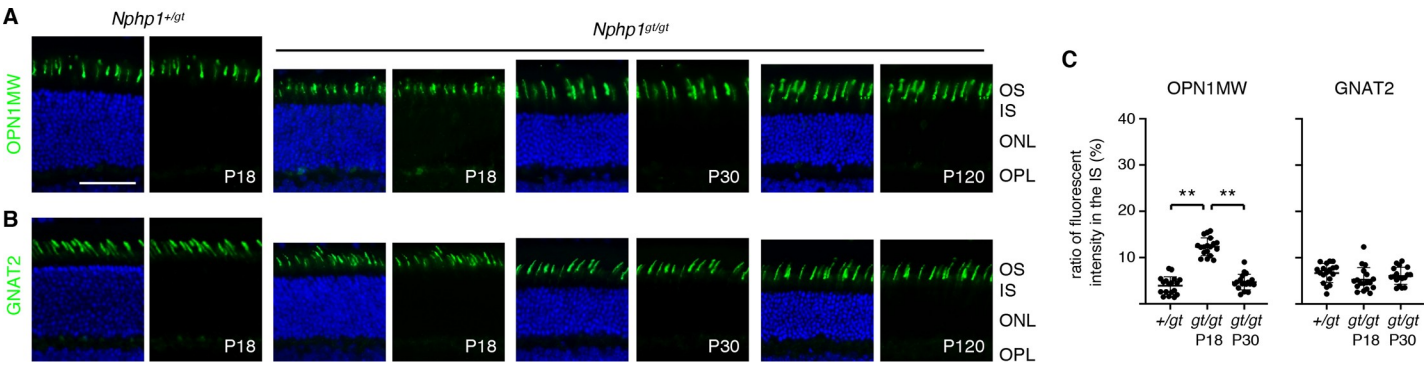

Fig 2. Localization of cone OS proteins in *Nphp1*$^{gt/gt}$ retinas. (A-B) Cone OS proteins, OPN1MW (A) and GNAT2 (B), were immunostained in *Nphp1*$^{+/gt}$ and *Nphp1*$^{gt/gt}$ retinal sections. Mild mislocalization of OPN1MW was observed at P18 but not at P30 in *Nphp1*$^{gt/gt}$ retinas. Scale bar denotes 50 μm. (C) Quantification of cone OS protein mislocalization to the IS. Others are the same as in Fig 1E.

https://doi.org/10.1371/journal.pone.0246358.g002

We then examined whether IS membrane proteins progressively accumulated in the OS as in *Cep290* mutant retinas [25]. To our surprise, localization of all proteins examined (STX3, STXBP1, SNAP25, and IMPG2) was significantly improved in 30-day old *Nphp1*$^{gt/gt}$ mutants and only a subset of photoreceptors displayed mislocalization (P30 in **Fig 1A–1E**). Localization of these proteins was even further improved by P60 and became indistinguishable from normal controls by P120. Mislocalization of RHO, PRPH2, ROM1, ABCA4, and PDE6B was not detected after P30 (**Fig 1 and S3 Fig**). OSs were also significantly elongated at P30 compared to P18 (21.27 ± 1.87 μm at P30 vs. 14.00 ± 1.53 μm at P18; n = 4; $p < 0.01$) (**Fig 1F**).

To test whether loss of NPHP1 more preferentially affects cone OS proteins, we examined the localization of OPN1MW (cone opsin) and GNAT2 (cone transducin α) in *Nphp1*$^{gt/gt}$ mutants (**Fig 2**). In 18-day old *Nphp1*$^{gt/gt}$ mice, cone OSs appeared to be short and disorganized. OPN1MW mostly localized to the OS but a small proportion was found mislocalized to the IS (**Fig 2A and 2C**). In contrast, localization of GNAT2 was not altered in *Nphp1*$^{gt/gt}$ retinas (**Fig 2B and 2C**). At P30 and P120, cone OSs appeared to be normal in length and shape, and no mislocalization of cone OS proteins was detected.

Retinal degeneration in *Nphp1*$^{gt/gt}$ mice

We examined photoreceptor degeneration in *Nphp1*$^{gt/gt}$ mutants. To this end, we counted the number of rows of photoreceptor cell nuclei at the central retina (300–600 μm from the optic nerve head). Consistent with the previous finding [22], there was a slight loss (~1 row) of photoreceptor cells by P18 (mean ± SD: 12.7 ± 0.7 in *Nphp1*$^{+/gt}$ vs. 11.6 ± 0.9 in *Nphp1*$^{gt/gt}$; $p<0.01$; n = 4) (**Fig 1G**). Thinning of the outer nuclear layer became more obvious and 3–4 rows of photoreceptors were lost by P30 (mean ± SD: 9.1 ± 0.9 at P30; $p<0.01$ compared with *Nphp1*$^{gt/gt}$ at P18; n = 4). However, retinal degeneration stopped thereafter and ~70% of photoreceptors were retained until 4 months of age (the last time point examined) in *Nphp1*$^{gt/gt}$ mice (8.8 ± 0.9 at P60 and 8.6 ± 0.8 at P120; n = 4) (**Fig 1G**).

Light response of *Nphp1*$^{gt/gt}$ mouse retinas

We next examined the capacity of *Nphp1*$^{gt/gt}$ mouse retinas to respond to light. In both dark- and light-adapted conditions and regardless of the stimulus light intensities, ERG b-wave amplitudes of 2-month-old *Nphp1*$^{gt/gt}$ mice were comparable to those of control animals (n = 4 per genotype; **Fig 3**). These data indicate that retinal functions of adult *Nphp1*$^{gt/gt}$ mice are largely unaffected by the gene-trap mutation.

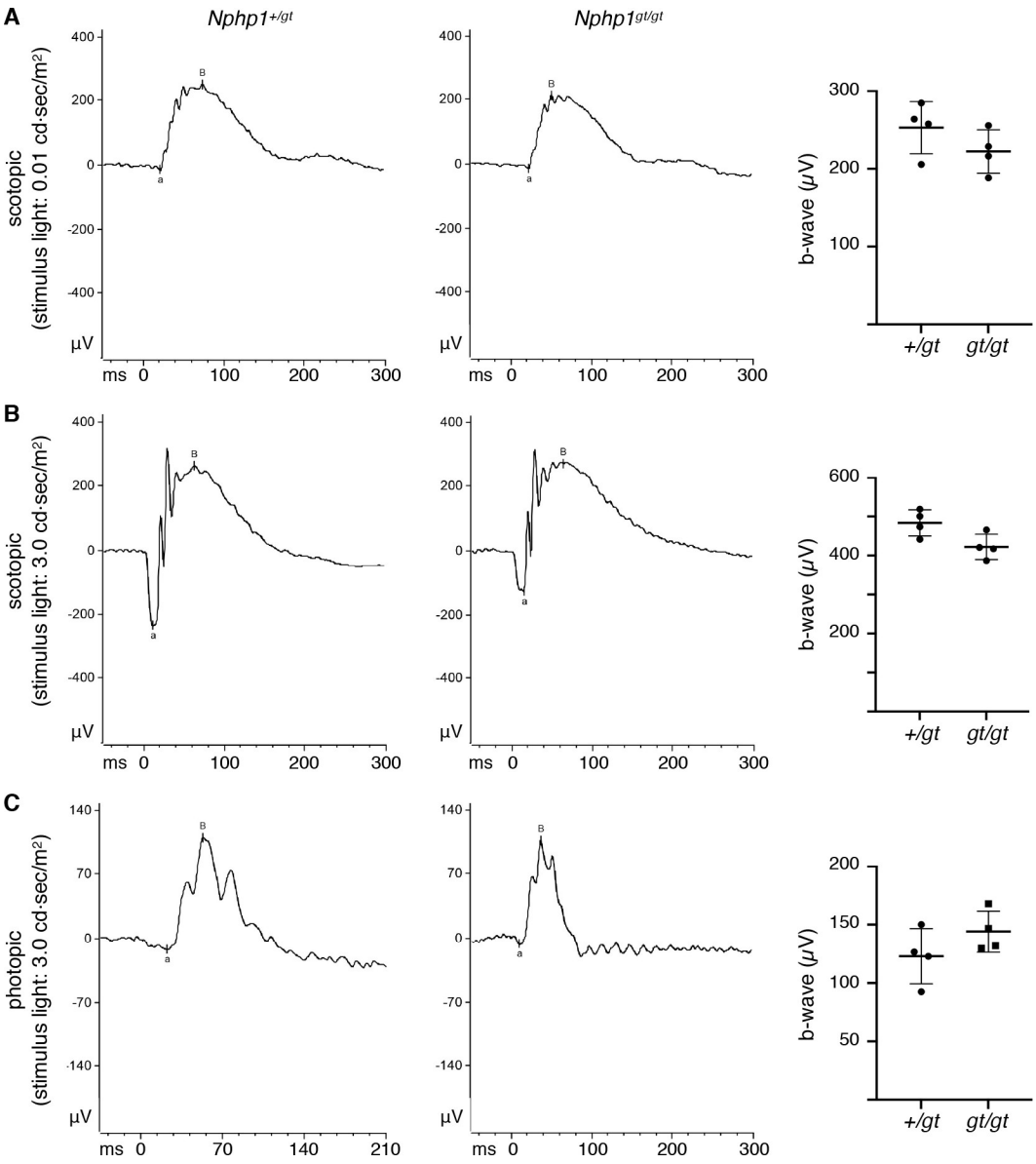

Fig 3. ERG responses of *Nphp1*$^{gt/gt}$ mouse retinas. Representative scotopic (A and B) and photopic (C) ERG recordings (average of 15 responses) from 2-month-old *Nphp1*$^{+/gt}$ and *Nphp1*$^{gt/gt}$ mice are shown. Stimulus light intensities are shown on the left. Each data point in the scatter plots (right) represents the average of ERG b-wave amplitudes of two eyes from individual animals (n = 4). Means ± SD are marked by horizontal lines. Scotopic ERGs were obtained with (A) 0.01 cd·sec/m^2 and (B) 3.0 cd·sec/m^2 flashes after overnight dark adaptation. Photopic ERGs (C) were obtained with 3.0 cd·sec/m^2 flashes in the presence of 9.0 cd·sec/m^2 background light after 10 minutes of light adaptation.

https://doi.org/10.1371/journal.pone.0246358.g003

Production of functional mRNAs from the *Nphp1*^{gt} allele

Spontaneous amelioration of protein mislocalization and retinal degeneration in *Nphp1*$^{gt/gt}$ mice sharply contrast with the severe retinal degeneration phenotype observed in *Nphp1*$^{del20/del20}$ mice [5]. To gain insights into the molecular basis of these striking differences, we examined possible expression of normal or mutant variants of NPHP1 in *Nphp1*$^{gt/gt}$ mice. More specifically, we directed our attention to non-canonical mRNA splicing events that could result in the production of functional proteins. Basal exon skipping and nonsense-associated altered

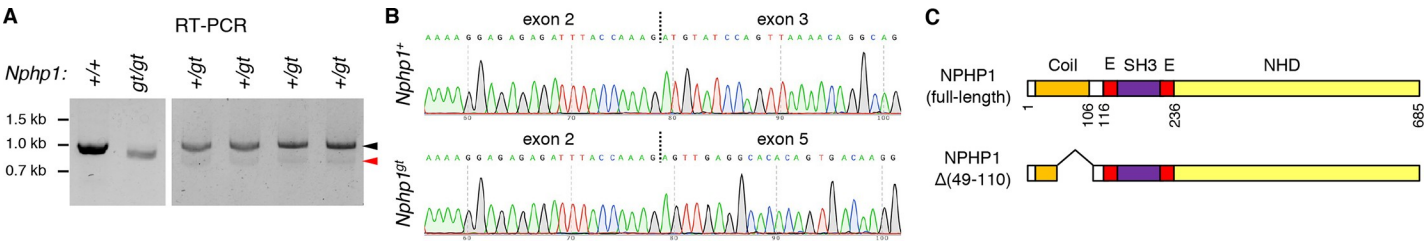

Fig 4. A small quantity of functional mRNA is produced from the *Nphp1*^{gt} allele via nonsense-associated altered splicing. (A) *Nphp1* RT-PCR data from *Nphp1*$^{+/+}$, *Nphp1*$^{gt/gt}$, and *Nphp1*$^{+/gt}$ retinas. Black and red arrowheads indicate PCR products from the wild-type and the *Nphp1*^{gt} allele, respectively. Each animal's *Nphp1* genotype is shown at the top. Locations of DNA size markers are shown on the left. (B) Chromatogram of RT-PCR product sequencing reactions around exon-exon junctions. Vertical dotted lines indicate exon-exon junctions. (C) Schematic representation of NPHP1 protein products encoded by wild-type and *Nphp1*^{gt} alleles. Major structural domains are depicted (Coil: coiled-coil domain; E: Glu-rich domain; SH3: SH3 domain; NHD: nephrocystin homology domain). Amino acid positions are shown below full-length NPHP1 and based on the translated amino acid sequence of BC118953.

https://doi.org/10.1371/journal.pone.0246358.g004

splicing are mechanisms, through which cells eliminate nonsense or frameshift mutation-containing exons during the pre-mRNA splicing. The resulting mRNAs maintain the reading frame of the gene and produce near-full-length proteins [44–49]. Neighboring exon(s) may be skipped as well if omitting the mutated exon alone does not prevent frameshift. These non-canonical splicing events have been reported in the human *CEP290* gene and account for the unexpectedly mild phenotypes observed in certain *CEP290*-LCA patients [46–49]. We recently showed that nonsense-associated altered splicing also occurs in a mouse model of *CEP290*-LCA [25]. The *Nphp1*^{gt} allele was generated by an insertion of a gene-trap into exon 4 (**S1 Fig**) [22], and we examined whether altered splicing occurred in *Nphp1*$^{gt/gt}$ mice.

To assess exon skipping, RNAs were extracted from 1.5-month-old *Nphp1*$^{+/+}$ and *Nphp1*$^{gt/gt}$ mouse eyes, and cDNA fragments were PCR-amplified using primers specific to *Nphp1* exons 2 and 11 (forward and reverse primers, respectively). In *Nphp1*$^{+/+}$ mice, a single PCR product containing all exons between exons 2 and 11 was amplified (991 bp; based on the transcript ID ENSMUST00000028857.13) (**Fig 4A**; left), suggesting no basal exon skipping. A slightly smaller fragment (805 bp) was amplified from *Nphp1*$^{gt/gt}$ mice. Sequence analyses of these PCR products revealed that the 805-bp fragment contained *Nphp1* coding sequences but lacked exons 3 and 4 as well as the gene-trap (**Fig 4B**). These data indicate that the entire gene-trap and *Nphp1* exons 3 and 4 were skipped during pre-mRNA splicing. *Nphp1* exons 3 and 4 are 61 bp and 125 bp long, respectively. Skipping of these two exons results in an in-frame deletion of 62 amino acids (aa; from Cys49 to Lys110 (p.C49_K110del)) within the N-terminal coiled-coil domain (**Fig 4C**). These data demonstrate that nonsense-associated altered splicing does occur in *Nphp1*^{gt} transcripts.

We noticed that the band intensity of the 805-bp fragment was significantly lower than that of wild-type fragments (**Fig 4A**; left). To better assess the quantity of *Nphp1*^{gt} mRNAs produced by nonsense-associated altered splicing, we performed PCR using cDNAs from *Nphp1*$^{+/gt}$ heterozygous mice and stopped PCR amplification after 30 cycles (i.e., before saturation) (**Fig 4A**; right). Using wild-type bands as an internal control, densitometric analysis of the PCR products indicated that the quantity of *Nphp1*^{gt} altered splicing products was less than 10% of wild-type mRNAs (mean ± SD: 6.3 ± 1.0%; n = 4). To test whether the nonsense-associated altered splicing is an age-dependent phenomenon and underlies the temporary retinal phenotypes, RNAs were extracted from 10-day old *Nphp1*$^{+/+}$, *Nphp1*$^{gt/gt}$, and *Nphp1*$^{+/gt}$ mouse eyes, and RT-PCR was conducted using the same PCR primers. RT-PCR results from young animals were similar to those of adult mice (**S4 Fig**), indicating that nonsense-associated altered splicing occurs similarly in both developing and matured retinas. We also examined whether *Nphp1* was differentially expressed during the retinal development. Quantitative

RT-PCR (qRT-PCR) data showed a minor difference in *Nphp1* transcript levels between mature and developing retinas (1.0 ± 0.02 at P30 vs. 0.84 ± 0.9 at P10, unpaired two-tailed *t* test, $p = 0.031$; S5 Fig). These data indicate that *Nphp1* expression does not change considerably during the retinal development.

Expression and localization of the NPHP1 deletion mutant encoded by the *Nphp1^{gt}* allele

We characterized the NPHP1 mutant protein encoded by the *Nphp1^{gt}* allele (hereafter NPHP1 Δ(49–110)). With the antibodies available to us, we were not able to detect endogenous NPHP1 convincingly in the retina by immunoblotting and immunohistochemistry. Therefore, we used protein extracts from testes, in which ciliary proteins were enriched (Fig 5A). While full-length NPHP1 with a calculated molecular weight of 77 kDa was readily detected in *Nphp1$^{+/+}$* testes (red arrowhead), we were not able to detect any unique protein band in *Nphp1$^{gt/gt}$* testes. The immunogen of our NPHP1 antibody corresponds to aa 345–614 of human NPHP1 and this region is intact in the NPHP1 Δ(49–110) mutant. Therefore, the lack of signal in *Nphp1$^{gt/gt}$* mutants is unlikely due to the lack of the epitope(s) in the mutant protein. Indeed, transfected HA-NPHP1 (full-length) and HA-NPHP1 Δ(49–110) mutants were equally well detected by both HA and NPHP1 antibodies (Fig 5B). These data indicate that the quantity of NPHP1 Δ(49–110) in *Nphp1$^{gt/gt}$* mutants is below the detection limit of our antibodies.

We then examined whether the 62-aa deletion in the coiled-coil domain affected the localization of NPHP1. To this end, we transfected HA-NPHP1 and HA-NPHP1 Δ(49–110) expression vectors to mIMCD-3 cells and examined their localization using HA antibodies (Fig 5C). Cilia and basal bodies were marked by ARL13B and γ-tubulin antibodies, respectively. As shown in Fig 5C, both full-length and Δ(49–110) mutant proteins localized to the transition zone in mIMCD-3 cells. These data indicate that the mutant protein retains its ability to localize to the transition zone.

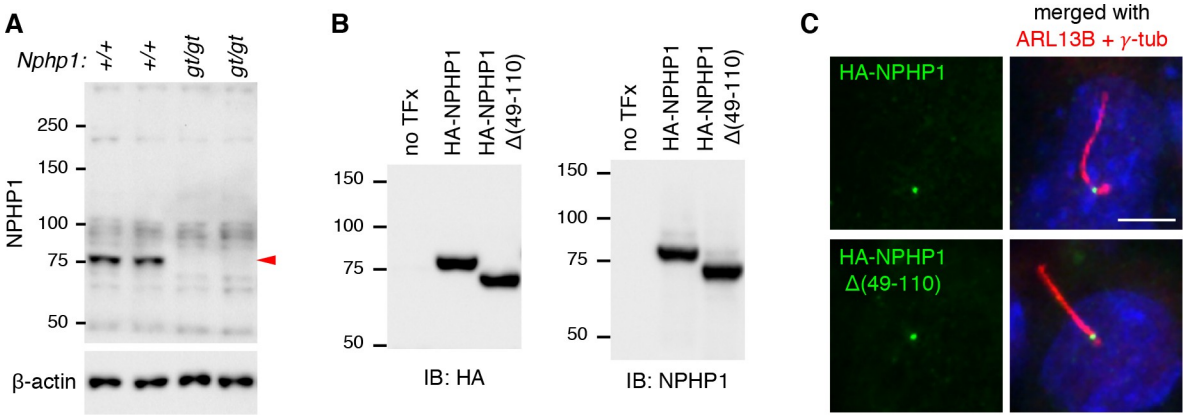

Fig 5. Expression and localization of NPHP1 Δ(49–110) deletion mutants. (A) Immunoblotting of NPHP1 (red arrowhead) in 35-day-old *Nphp1$^{+/+}$* and *Nphp1$^{gt/gt}$* mouse testes. Fifty μg of proteins were loaded per lane. β-actin was used as a loading control. (B) Expression of HA-tagged NPHP1 and NPHP1 Δ(49–110) in transiently transfected 293T/17 cells. Cell lysates were subjected to SDS-PAGE and immunoblotting (IB) with anti-HA and anti-NPHP1 antibodies. (C) Localization of NPHP1 Δ(49–110) to the transition zone in mIMCD-3 cells. HA-NPHP1 and HA-NPHP1 Δ(49–110) were transiently transfected to mIMCD-3 cells and their localization was probed with anti-HA antibodies (green). ARL13B and γ-tubulin (red) were immuno-labeled to mark primary cilia and basal bodies, respectively. DAPI (blue) was used to counterstain the nuclei. Scale bar represents 2 μm.

https://doi.org/10.1371/journal.pone.0246358.g005

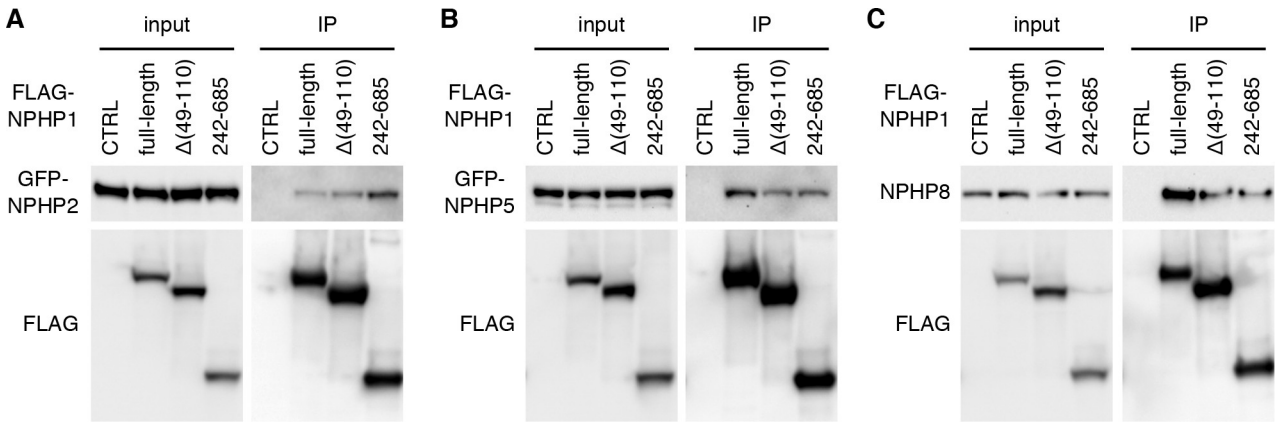

Fig 6. Interaction of NPHP1 Δ(49–110) with other NPHP proteins. Expression vectors of FLAG-tagged NPHP1 (full-length), NPHP1 Δ(49–110), and NPHP1 aa242-685 were co-transfected with either pEGFP-NPHP2 (A) or pEGFP-NPHP5 (B) to 293T/17 cells, and protein extracts were subjected to immunoprecipitation (IP) with anti-FLAG antibodies. Empty vectors were used as a negative control (CTRL). For NPHP8 (C), endogenous NPHP8 was probed.

https://doi.org/10.1371/journal.pone.0246358.g006

NPHP1 Δ(49–110) mutants retain the ability to interact with other NPHP proteins

We next examined whether the deletion had any impact on protein-protein interactions of NPHP1. NPHP1 is previously shown to interact with AHI1, NPHP2 (also known as INVS), NPHP4, NPHP5 (IQCB1), and NPHP8 (RPGRIP1L) [10, 50–53]. Of these, NPHP1 directly binds to AHI1 and NPHP4 via its SH3 domain and the C-terminal 131 residues, respectively [10, 50, 52, 53]. Since these regions are preserved in the NPHP1 Δ(49–110) mutant and sufficient to mediate NPHP1 interactions with AHI1 and NPHP4, we focused our efforts on interactions with NPHP2, NPHP5, and NPHP8. To this end, we transiently transfected FLAG-tagged NPHP1 variants (full-length NPHP1, NPHP1 Δ(49–110), and NPHP1 aa242-685) with GFP-tagged NPHP2 and NPHP5, and performed immunoprecipitation (IP) using anti-FLAG antibodies (**Fig 6**). For NPHP8, endogenous proteins were probed. As shown in **Fig 6**, both NPHP1 Δ(49–110) and NPHP1 aa242-685 were able to pull down all three NPHP proteins, indicating that the C-terminal nephrocystin homology domain (NHD) alone was sufficient to interact with these proteins either directly or indirectly. These data show that the NPHP1 Δ(49–110) mutant retains most, if not all, of its protein-protein interaction capabilities.

Cep290 genetically interacts with *Nphp1* and modifies retinal phenotypes in *Nphp1*$^{gt/gt}$ mice

Finally, we tested whether additional mutations in other ciliary gate-related genes could modify the severity of retinal degeneration in *Nphp1*$^{gt/gt}$ mice. To this end, we crossed *Nphp1*$^{gt/gt}$ mice to *Cep290*$^{fl/fl}$;*iCre75* mice [25, 30, 31] and compared protein mislocalization and retinal degeneration phenotypes in *Nphp1*$^{gt/gt}$;*Cep290*$^{+/+}$;*iCre75* and *Nphp1*$^{gt/gt}$;*Cep290*$^{+/fl}$;*iCre75* animals: all animals analyzed in this study were *iCre75* hemizygotes and *iCre75* genotype is omitted for brevity. At 1 month of age, mislocalization of IS plasma membrane proteins STX3, STXBP1, and SNAP25 was significantly increased in *Nphp1*$^{gt/gt}$;*Cep290*$^{+/fl}$ mice compared with that in *Nphp1*$^{gt/gt}$;*Cep290*$^{+/+}$ mice (**Fig 7**). RHO mislocalization was also detected in *Nphp1*$^{gt/gt}$;*Cep290*$^{+/fl}$ mice, but it was relatively mild compared to that of IS membrane proteins. Consistent with the increased protein mislocalization, reduction of the outer nuclear layer was evident in *Nphp1*$^{gt/gt}$;*Cep290*$^{+/fl}$ mice. At 2 months of age, when *Nphp1*$^{gt/gt}$;*Cep290*$^{+/+}$ mice

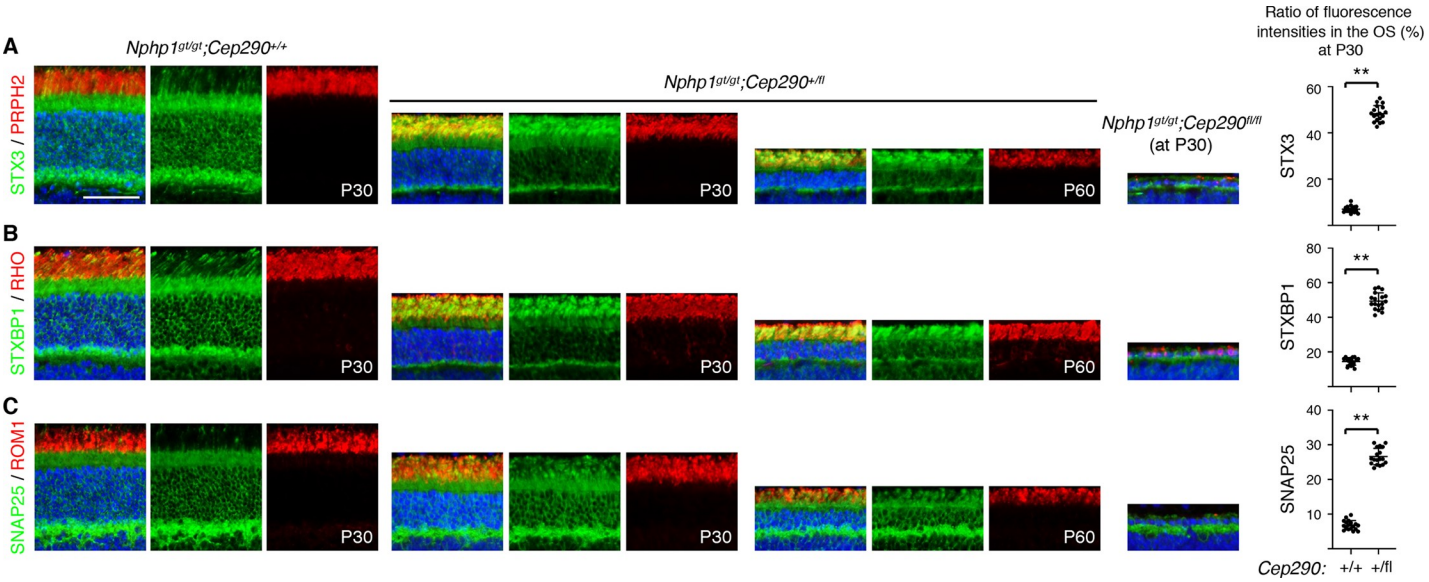

Fig 7. Genetic interaction of *Nphp1* with *Cep290*. Mislocalization of STX3 (A), STXBP1 (B), and SNAP25 (C) in $Nphp^{gt/gt}$;$Cep290^{+/+}$, $Nphp^{gt/gt}$;$Cep290^{+/fl}$, and $Nphp^{gt/gt}$;$Cep290^{fl/fl}$ retinas (green). PRPH2, RHO, and ROM1 (red) were labeled to mark the OS. The ratio of mislocalized proteins was quantified as in Fig 1 and depicted on the right. Mean ± SD is marked by horizontal lines (n = 3 mice; 2 sections/mouse and 3 areas/section). Asterisks indicate statistical significance (unpaired, 2-tailed *t* test; $p < 0.01$).

https://doi.org/10.1371/journal.pone.0246358.g007

exhibited no mislocalization and no degeneration, $Nphp1^{gt/gt}$;$Cep290^{+/fl}$ mice exhibited severe retinal degeneration with only 3–5 rows of photoreceptor cell nuclei remaining. In $Nphp1^{gt/gt}$;$Cep290^{fl/fl}$ double mutants, more than 90% of photoreceptors were lost by P30, which is faster than what we observed in $Cep290^{fl/fl}$ single mutants using the same *Cre* driver [25]. These data indicate that *Nphp1* and *Cep290* genetically interact and that reduction of *Cep290* gene dose exacerbates protein confinement defects and causes continuous retinal degeneration in $Nphp1^{gt/gt}$ mice.

Discussion

In this work, we characterize retinal degeneration in a mouse model of NPHP1 and demonstrate the requirement of NPHP1 for compartmentalized protein localization in photoreceptors. The mutant allele in the $Nphp1^{gt}$ model is likely a hypomorph rather than a null because of the production of a small number of functional mRNAs derived from nonsense-associated altered splicing. The resulting mRNAs encode a near-full-length protein with a 62-aa in-frame deletion. The mutant protein appears to retain most, if not all, functions of the full-length protein, as it correctly localizes to the ciliary transition zone and interacts with its known binding partners. However, the quantity of the functional mRNAs produced by altered splicing is very low (less than 10% of wild type), and the protein products are below the detection limit with the reagents available to us. Although we were not able to detect the mutant protein in the testis, it is noteworthy that all $Nphp1^{gt/gt}$ males (n = 12) used for breeding produced offspring with normal litter size (5–12 pups/litter). This is contrary to the sterility of $Nphp1^{del20/del20}$ males [21]. Therefore, our data suggest that the $Nphp1^{gt}$ allele is a hypomorph and that the phenotypic differences between the two NPHP1 mouse models are due to a difference in the residual activities of the two mutant alleles rather than their genetic backgrounds.

Our study shows that NPHP1 is involved in membrane protein confinement at the connecting cilium. In developing $Nphp1^{gt/gt}$ retinas, confinement of IS plasma membrane proteins is

compromised, leading to an infiltration of IS membrane proteins into the OS. Among the OS proteins examined, only opsins (RHO and OPN1MW) showed mislocalization to the IS and the degree of mislocalization was relatively mild compared to that of IS plasma membrane proteins. This phenotype is very similar to what is observed in *Cep290*^{fl} mice [25]. It also should be noted that, despite more severe RHO mislocalization and faster degeneration, IS membrane protein mislocalization does not occur in *Ift88* mutants (**S6 Fig**). These data suggest that IS membrane protein mislocalization is not a consequence of the degenerative process occurring in dying cells. Therefore, although it has been examined in only two disease models thus far, our findings are consistent with the idea that accumulation of IS membrane proteins in the OS is a common pathomechanism of retinal degenerations associated with ciliary gate defects [3]. Further investigation is needed to validate this idea in other ciliary gate-related retinal degenerations. It is also noteworthy that although Bardet-Biedl syndrome (BBS) proteins are not part of the ciliary gate complex, retinal degeneration in BBS shares the same disease mechanism [38, 54, 55]. Future studies should be directed towards discovering how this molecular phenotype leads to the death of photoreceptor cells.

Interestingly, however, the requirement of NPHP1 in photoreceptors is developmental stage dependent. In mice, the connecting cilium assembles at P3-5 and the OS develops afterward until P18-20 [56, 57]. Protein mislocalization occurs in *Nphp1*$^{gt/gt}$ retinas when OSs are actively elongating, but normal distribution patterns are restored after P18. Some photoreceptors die during this period, but retinal degeneration stops as the protein confinement defect is ameliorated. Retinal functions and anatomy appear to be normal in adult *Nphp1*$^{gt/gt}$ mice except ~30% thinner ONL due to the earlier loss of photoreceptors. RT-PCR data indicate that nonsense-associated altered splicing of *Nphp1*^{gt} pre-mRNAs occurs in not only fully matured but also developing retinas. Therefore, age-dependent differences in altered splicing are not likely a contributing factor. One speculation is that, although ciliary gate functions are essential throughout the life of photoreceptors, more vigorous NPHP1 activities might be needed when OSs are rapidly elongating compared to when the OS elongation is completed. Further studies are warranted on this topic.

Our study suggests that additional mutations in other ciliary gate-related genes may affect the penetrance of retinopathy in human NPHP1 patients. As mentioned in the Introduction, only 6–10% of NPHP1 patients manifest retinal anomalies [19, 20, 58]. The most frequent mutations in human *NPHP1*, found in 65–80% of NPHP1 patients, are large (~250 kb) homozygous deletions that eliminate the majority of *NPHP1* exons [16–18, 59]. Since these mutations are expected to be null, NPHP1 does not appear to be essential for photoreceptor health in humans. A previous study showed that removal of one allele of *Ahi1*, which encodes a component of the ciliary gate complex [10], significantly increases RHO mislocalization and accelerates retinal degeneration in *Nphp1*$^{gt/gt}$ mice [22]. In the present work, we show that reducing the gene dose of *Cep290* in *Nphp1*$^{gt/gt}$ mice exacerbates protein mislocalization and causes retinal degeneration that continues in mature retinas. These findings suggest that *NPHP1* genetically interacts with other ciliary gate-related genes and that the manifestation of retinopathy in NPHP1 patients may be affected by the presence of additional mutations in those genes.

Our study also suggests that mutation-induced non-canonical splicing might be more common than what has been appreciated. As mentioned above, some *CEP290*-LCA patients exhibit relatively mild phenotypes despite the presence of truncation mutations that should eliminate a large proportion of the protein [46–49]. The unexpectedly mild phenotypes are due to the production of near-full-length proteins derived from non-canonical mRNA splicing that skips exons with truncating mutations. One of the interesting features of inherited retinal degenerations is the wide spectrum of phenotypic severity despite mutations in the same gene [20, 60–66]. Although some of these variations can be explained by disease-causing mutations

per se (e.g. missense mutations that partly reduce protein activities) and genetic modifiers, nonsense-associated altered splicing may contribute to the variation and underlie the mild end of the phenotypic spectrum of disease.

Finally, our study urges a more thorough investigation of mRNAs produced in mutant animals. When loss-of-function animal models are generated, inducing frameshift is a frequently used strategy. For example, CRISPR-based gene knockout approaches utilize the tendency of introducing indels at double-strand breaks, which results in a frameshift. In more conventional recombination-based approaches, exons, deletion of which causes frameshift, are preferentially selected when designing targeting vectors. Accumulating evidence indicates that exons containing premature termination codons are often skipped as a compensatory mechanism to cope with induced mutations [67–69]. Our results show that gene-traps can be skipped as well during splicing. Therefore, a thorough investigation of mRNAs produced from mutant alleles is warranted before beginning extensive studies and making conclusions without knowing the precise consequences of the mutation.

Conclusions

Our study shows that NPHP1 is required to maintain compartmentalized protein localization during the photoreceptor terminal differentiation, particularly to prevent infiltration of IS plasma membrane proteins into the OS. However, this requirement is developmental stage-dependent, and NPHP1 becomes less crucial as the OS elongation is completed. Retinal degeneration occurs when NPHP1 deficiency causes protein mislocalization but stops as normal localization patterns are restored. These findings suggest that accumulation of IS membrane proteins in the OS is part of the disease mechanisms underlying the *NPHP1*-associated retinopathy. Our study further shows that reduction of *Cep290* gene dose exacerbates protein confinement defects and retinal degeneration in *Nphp1* mutants. These findings suggest that additional mutations in other ciliary gate-related genes may influence the penetrance of retinopathy in human NPHP1 patients.

Supporting information

S1 Fig. Schematics of mouse *Nphp1* wild-type and gene-trap (gt) alleles. Black boxes represent *Nphp1* exons. Exon numbers are described above the black boxes. The PGK-Neo gene-trap is inserted into *Nphp1* exon 4. PGK: mouse phosphoglycerate kinase 1 promoter, Neo: neomycin resistance gene, pA: poly(A) signal.
(TIF)

S2 Fig. Validation of the RPGRIP1L antibody. hTERT-RPE1 cells (ATCC #CRL-4000) were transfected with control (siCTRL; Horizon ON-TARGETplus Non-targeting Pool cat#: D-001810-10-05) or human RPGRIP1L siRNAs (siRPGRIP1L; Horizon ON-TARGETplus SMARTpool cat# L-022557-00-0005) using Lipofectamine RNAiMAX (Invitrogen), and cell lysates were loaded on an SDS-PAGE gel for immunoblotting with anti-RPGRIP1L antibodies. β-actin was used as a loading control. RPGRIP1L band was marked with a red arrowhead.
(TIF)

S3 Fig. Localization of OS resident proteins in *Nphp1*$^{gt/gt}$ retinas. (A-C) Localization of RHO (A), ABCA4 (B), and PDE6B (C) in *Nphp1*$^{gt/gt}$ retinas. Retinal sections from *Nphp1*$^{+/gt}$ and *Nphp1*$^{gt/gt}$ mice were stained with RHO, ABCA4, and PDE6B antibodies (red). DAPI (blue) was used to counterstain the nuclei. Mild mislocalization of RHO was detected in *Nphp1*$^{gt/gt}$ retinas at P18. Localization of ABCA4 and PDE6B was not affected. Scale bar denotes 50 μm. (D) Quantification of RHO mislocalization to the IS. Depicted is the ratio of

integrated fluorescence intensity in the IS relative to the photoreceptor cell layer. Mean ± SD (error bars) is marked by horizontal lines (n = 3 mice; 2 sections/mouse and 3 areas/section). Asterisks indicate statistical significance (one-way ANOVA followed by Tukey's multiple comparison test; $p < 0.01$).
(TIFF)

S4 Fig. *Nphp1* RT-PCR data from 10-day-old *Nphp1*$^{+/+}$, *Nphp1*$^{gt/gt}$, and *Nphp1*$^{+/gt}$ mouse retinas.
(TIF)

S5 Fig. *Nphp1* expression levels in developing and mature retinas. RNAs were extracted from *Nphp1*$^{+/+}$ mouse retinas at P30 (n = 3) and P6 (n = 4), and relative *Nphp1* mRNA levels were determined by qRT-PCR.
(TIF)

S6 Fig. Depletion of IFT88 does not cause IS membrane protein accumulation in the OS. Retinal sections from 30-day and 40-day old *Ift88*$^{fl/fl}$*;iCre75* mice were stained with STX3 (A) and STXBP1 (B) antibodies (green). PRPH2 and RHO (red) were labeled as a marker of the OS. Merged images are shown on the left in each set. DAPI (blue) was used to counterstain the nuclei. Scale bar denotes 50 μm.
(TIF)

S1 File. Raw images.
(PDF)

Acknowledgments

The authors thank Drs. Val C. Sheffield (University of Iowa, USA) and William Y. Tsang (Institut de Recherches Cliniques de Montreal, Canada) for the gifts of pEGFP-NPHP2 and pEGFP-NPHP5, respectively.

Author Contributions

Conceptualization: Seongjin Seo.

Data curation: Seongjin Seo.

Formal analysis: Poppy Datta, J. Thomas Cribbs, Seongjin Seo.

Funding acquisition: Seongjin Seo.

Investigation: Poppy Datta, J. Thomas Cribbs.

Methodology: Poppy Datta, J. Thomas Cribbs.

Project administration: Seongjin Seo.

Supervision: Seongjin Seo.

Validation: Poppy Datta, J. Thomas Cribbs.

Visualization: Poppy Datta, Seongjin Seo.

Writing – original draft: Seongjin Seo.

Writing – review & editing: Poppy Datta, J. Thomas Cribbs.

References

1. Pearring JN, Salinas RY, Baker SA, Arshavsky VY. Protein sorting, targeting and trafficking in photoreceptor cells. Progress in retinal and eye research. 2013; 36:24–51. https://doi.org/10.1016/j.preteyeres.2013.03.002 PMID: 23562855; PubMed Central PMCID: PMC3759535.
2. Baehr W, Hanke-Gogokhia C, Sharif A, Reed M, Dahl T, Frederick JM, et al. Insights into photoreceptor ciliogenesis revealed by animal models. Progress in retinal and eye research. 2019; 71:26–56. Epub 2018/12/28. https://doi.org/10.1016/j.preteyeres.2018.12.004 PMID: 30590118; PubMed Central PMCID: PMC6707082.
3. Seo S, Datta P. Photoreceptor outer segment as a sink for membrane proteins: hypothesis and implications in retinal ciliopathies. Hum Mol Genet. 2017; 26(R1):R75–R82. https://doi.org/10.1093/hmg/ddx163 PMID: 28453661; PubMed Central PMCID: PMC5886464.
4. Fliegauf M, Horvath J, von Schnakenburg C, Olbrich H, Muller D, Thumfart J, et al. Nephrocystin specifically localizes to the transition zone of renal and respiratory cilia and photoreceptor connecting cilia. J Am Soc Nephrol. 2006; 17(9):2424–33. Epub 2006/08/04. https://doi.org/10.1681/ASN.2005121351 PMID: 16885411.
5. Jiang ST, Chiou YY, Wang E, Chien YL, Ho HH, Tsai FJ, et al. Essential role of nephrocystin in photoreceptor intraflagellar transport in mouse. Hum Mol Genet. 2009; 18(9):1566–77. Epub 2009/02/12. https://doi.org/10.1093/hmg/ddp068 PMID: 19208653.
6. Schermer B, Hopker K, Omran H, Ghenoiu C, Fliegauf M, Fekete A, et al. Phosphorylation by casein kinase 2 induces PACS-1 binding of nephrocystin and targeting to cilia. EMBO J. 2005; 24(24):4415–24. Epub 2005/11/26. https://doi.org/10.1038/sj.emboj.7600885 PMID: 16308564; PubMed Central PMCID: PMC1356326.
7. Seeger-Nukpezah T, Liebau MC, Hopker K, Lamkemeyer T, Benzing T, Golemis EA, et al. The centrosomal kinase Plk1 localizes to the transition zone of primary cilia and induces phosphorylation of nephrocystin-1. PLoS One. 2012; 7(6):e38838. Epub 2012/06/16. https://doi.org/10.1371/journal.pone.0038838 PMID: 22701722; PubMed Central PMCID: PMC3372538.
8. Garcia-Gonzalo FR, Corbit KC, Sirerol-Piquer MS, Ramaswami G, Otto EA, Noriega TR, et al. A transition zone complex regulates mammalian ciliogenesis and ciliary membrane composition. Nature genetics. 2011; 43(8):776–84. Epub 2011/07/05. https://doi.org/10.1038/ng.891 PMID: 21725307; PubMed Central PMCID: PMC3145011.
9. Shi X, Garcia G 3rd, Van De Weghe JC, McGorty R, Pazour GJ, Doherty D, et al. Super-resolution microscopy reveals that disruption of ciliary transition-zone architecture causes Joubert syndrome. Nat Cell Biol. 2017; 19(10):1178–88. Epub 2017/08/29. https://doi.org/10.1038/ncb3599 PMID: 28846093; PubMed Central PMCID: PMC5695680.
10. Sang L, Miller JJ, Corbit KC, Giles RH, Brauer MJ, Otto EA, et al. Mapping the NPHP-JBTS-MKS protein network reveals ciliopathy disease genes and pathways. Cell. 2011; 145(4):513–28. Epub 2011/05/14. https://doi.org/10.1016/j.cell.2011.04.019 PMID: 21565611.
11. Williams CL, Li C, Kida K, Inglis PN, Mohan S, Semenec L, et al. MKS and NPHP modules cooperate to establish basal body/transition zone membrane associations and ciliary gate function during ciliogenesis. The Journal of cell biology. 2011; 192(6):1023–41. Epub 2011/03/23. https://doi.org/10.1083/jcb.201012116 PMID: 21422230; PubMed Central PMCID: PMC3063147.
12. Garcia-Gonzalo FR, Reiter JF. Scoring a backstage pass: mechanisms of ciliogenesis and ciliary access. J Cell Biol. 2012; 197(6):697–709. Epub 2012/06/13. https://doi.org/10.1083/jcb.201111146 PMID: 22689651; PubMed Central PMCID: PMC3373398.
13. Garcia-Gonzalo FR, Reiter JF. Open Sesame: How Transition Fibers and the Transition Zone Control Ciliary Composition. Cold Spring Harb Perspect Biol. 2017; 9(2):10.1101/cshperspect.a028134. https://doi.org/10.1101/cshperspect.a028134 PMID: 27770015.
14. Hildebrandt F, Benzing T, Katsanis N. Ciliopathies. N Engl J Med. 2011; 364(16):1533–43. https://doi.org/10.1056/NEJMra1010172 PMID: 21506742; PubMed Central PMCID: PMC3640822.
15. Reiter JF, Leroux MR. Genes and molecular pathways underpinning ciliopathies. Nat Rev Mol Cell Biol. 2017; 18(9):533–47. Epub 2017/07/13. https://doi.org/10.1038/nrm.2017.60 PMID: 28698599; PubMed Central PMCID: PMC5851292.
16. Konrad M, Saunier S, Heidet L, Silbermann F, Benessy F, Calado J, et al. Large homozygous deletions of the 2q13 region are a major cause of juvenile nephronophthisis. Hum Mol Genet. 1996; 5(3):367–71. Epub 1996/03/01. https://doi.org/10.1093/hmg/5.3.367 PMID: 8852662.
17. Hildebrandt F, Otto E, Rensing C, Nothwang HG, Vollmer M, Adolphs J, et al. A novel gene encoding an SH3 domain protein is mutated in nephronophthisis type 1. Nat Genet. 1997; 17(2):149–53. Epub 1997/11/05. https://doi.org/10.1038/ng1097-149 PMID: 9326933.

18. Saunier S, Calado J, Heilig R, Silbermann F, Benessy F, Morin G, et al. A novel gene that encodes a protein with a putative src homology 3 domain is a candidate gene for familial juvenile nephronophthisis. Hum Mol Genet. 1997; 6(13):2317–23. Epub 1998/03/21. https://doi.org/10.1093/hmg/6.13.2317 PMID: 9361039.

19. Hildebrandt F, Attanasio M, Otto E. Nephronophthisis: disease mechanisms of a ciliopathy. J Am Soc Nephrol. 2009; 20(1):23–35. Epub 2009/01/02. https://doi.org/10.1681/ASN.2008050456 PMID: 19118152; PubMed Central PMCID: PMC2807379.

20. Caridi G, Murer L, Bellantuono R, Sorino P, Caringella DA, Gusmano R, et al. Renal-retinal syndromes: association of retinal anomalies and recessive nephronophthisis in patients with homozygous deletion of the NPH1 locus. Am J Kidney Dis. 1998; 32(6):1059–62. Epub 1998/12/18. https://doi.org/10.1016/s0272-6386(98)70083-6 PMID: 9856524.

21. Jiang ST, Chiou YY, Wang E, Lin HK, Lee SP, Lu HY, et al. Targeted disruption of Nphp1 causes male infertility due to defects in the later steps of sperm morphogenesis in mice. Hum Mol Genet. 2008; 17 (21):3368–79. Epub 2008/08/08. https://doi.org/10.1093/hmg/ddn231 PMID: 18684731.

22. Louie CM, Caridi G, Lopes VS, Brancati F, Kispert A, Lancaster MA, et al. AHI1 is required for photoreceptor outer segment development and is a modifier for retinal degeneration in nephronophthisis. Nat Genet. 2010; 42(2):175–80. https://doi.org/10.1038/ng.519 PMID: 20081859; PubMed Central PMCID: PMC2884967.

23. Yee LE, Garcia-Gonzalo FR, Bowie RV, Li C, Kennedy JK, Ashrafi K, et al. Conserved Genetic Interactions between Ciliopathy Complexes Cooperatively Support Ciliogenesis and Ciliary Signaling. PLoS Genet. 2015; 11(11):e1005627. Epub 2015/11/06. https://doi.org/10.1371/journal.pgen.1005627 PMID: 26540106; PubMed Central PMCID: PMC4635004.

24. Rao KN, Zhang W, Li L, Ronquillo C, Baehr W, Khanna H. Ciliopathy-associated protein CEP290 modifies the severity of retinal degeneration due to loss of RPGR. Hum Mol Genet. 2016; 25(10):2005–12. Epub 2016/03/05. https://doi.org/10.1093/hmg/ddw075 PMID: 26936822; PubMed Central PMCID: PMC5062589.

25. Datta P, Hendrickson B, Brendalen S, Ruffcorn A, Seo S. The myosin-tail homology domain of centrosomal protein 290 is essential for protein confinement between the inner and outer segments in photoreceptors. J Biol Chem. 2019; 294(50):19119–36. Epub 2019/11/07. https://doi.org/10.1074/jbc.RA119.009712 PMID: 31694913; PubMed Central PMCID: PMC6916492.

26. den Hollander AI, Koenekoop RK, Yzer S, Lopez I, Arends ML, Voesenek KE, et al. Mutations in the CEP290 (NPHP6) gene are a frequent cause of Leber congenital amaurosis. American journal of human genetics. 2006; 79(3):556–61. Epub 2006/08/16. https://doi.org/10.1086/507318 PMID: 16909394; PubMed Central PMCID: PMC1559533.

27. Sayer JA, Otto EA, O'Toole JF, Nurnberg G, Kennedy MA, Becker C, et al. The centrosomal protein nephrocystin-6 is mutated in Joubert syndrome and activates transcription factor ATF4. Nat Genet. 2006; 38(6):674–81. https://doi.org/10.1038/ng1786 PMID: 16682973.

28. Baala L, Audollent S, Martinovic J, Ozilou C, Babron MC, Sivanandamoorthy S, et al. Pleiotropic effects of CEP290 (NPHP6) mutations extend to Meckel syndrome. Am J Hum Genet. 2007; 81(1):170–9. https://doi.org/10.1086/519494 PMID: 17564974.

29. Cideciyan AV, Aleman TS, Jacobson SG, Khanna H, Sumaroka A, Aguirre GK, et al. Centrosomal-ciliary gene CEP290/NPHP6 mutations result in blindness with unexpected sparing of photoreceptors and visual brain: implications for therapy of Leber congenital amaurosis. Human mutation. 2007; 28 (11):1074–83. Epub 2007/06/08. https://doi.org/10.1002/humu.20565 PMID: 17554762.

30. Lancaster MA, Gopal DJ, Kim J, Saleem SN, Silhavy JL, Louie CM, et al. Defective Wnt-dependent cerebellar midline fusion in a mouse model of Joubert syndrome. Nat Med. 2011; 17(6):726–31. https://doi.org/10.1038/nm.2380 PMID: 21623382; PubMed Central PMCID: PMC3110639.

31. Li S, Chen D, Sauve Y, McCandless J, Chen YJ, Chen CK. Rhodopsin-iCre transgenic mouse line for Cre-mediated rod-specific gene targeting. Genesis. 2005; 41(2):73–80. https://doi.org/10.1002/gene.20097 PMID: 15682388.

32. Turner DL, Weintraub H. Expression of achaete-scute homolog 3 in Xenopus embryos converts ectodermal cells to a neural fate. Genes Dev. 1994; 8(12):1434–47. Epub 1994/06/15. https://doi.org/10.1101/gad.8.12.1434 PMID: 7926743.

33. Gimona M, Vandekerckhove J, Goethals M, Herzog M, Lando Z, Small JV. Beta-actin specific monoclonal antibody. Cell Motil Cytoskeleton. 1994; 27(2):108–16. Epub 1994/01/01. https://doi.org/10.1002/cm.970270203 PMID: 8162619.

34. Datta P, Ruffcorn A, Seo S. Limited time window for retinal gene therapy in a preclinical model of ciliopathy. Hum Mol Genet. 2020; 29(14):2337–52. Epub 2020/06/23. https://doi.org/10.1093/hmg/ddaa124 PMID: 32568387; PubMed Central PMCID: PMC7424757.

35. Illing M, Molday LL, Molday RS. The 220-kDa rim protein of retinal rod outer segments is a member of the ABC transporter superfamily. J Biol Chem. 1997; 272(15):10303–10. Epub 1997/04/11. https://doi.org/10.1074/jbc.272.15.10303 PMID: 9092582.

36. Molday LL, Rabin AR, Molday RS. ABCR expression in foveal cone photoreceptors and its role in Stargardt macular dystrophy. Nat Genet. 2000; 25(3):257–8. Epub 2000/07/11. https://doi.org/10.1038/77004 PMID: 10888868.

37. Humbert MC, Weihbrecht K, Searby CC, Li Y, Pope RM, Sheffield VC, et al. ARL13B, PDE6D, and CEP164 form a functional network for INPP5E ciliary targeting. Proceedings of the National Academy of Sciences of the United States of America. 2012; 109(48):19691–6. Epub 2012/11/15. https://doi.org/10.1073/pnas.1210916109 PMID: 23150559; PubMed Central PMCID: PMC3511769.

38. Datta P, Allamargot C, Hudson JS, Andersen EK, Bhattarai S, Drack AV, et al. Accumulation of non-outer segment proteins in the outer segment underlies photoreceptor degeneration in Bardet-Biedl syndrome. Proc Natl Acad Sci U S A. 2015; 112(32):E4400–9. https://doi.org/10.1073/pnas.1510111112 PMID: 26216965.

39. Salido EM, Ramamurthy V. Proteoglycan IMPG2 Shapes the Interphotoreceptor Matrix and Modulates Vision. J Neurosci. 2020; 40(20):4059–72. Epub 2020/04/09. https://doi.org/10.1523/JNEUROSCI.2994-19.2020 PMID: 32265257; PubMed Central PMCID: PMC7219290.

40. Beltran WA, Hammond P, Acland GM, Aguirre GD. A frameshift mutation in RPGR exon ORF15 causes photoreceptor degeneration and inner retina remodeling in a model of X-linked retinitis pigmentosa. Invest Ophthalmol Vis Sci. 2006; 47(4):1669–81. Epub 2006/03/28. https://doi.org/10.1167/iovs.05-0845 PMID: 16565408.

41. Rhee KD, Ruiz A, Duncan JL, Hauswirth WW, Lavail MM, Bok D, et al. Molecular and cellular alterations induced by sustained expression of ciliary neurotrophic factor in a mouse model of retinitis pigmentosa. Invest Ophthalmol Vis Sci. 2007; 48(3):1389–400. Epub 2007/02/28. https://doi.org/10.1167/iovs.06-0677 PMID: 17325188; PubMed Central PMCID: PMC7147570.

42. Molday RS, MacKenzie D. Monoclonal antibodies to rhodopsin: characterization, cross-reactivity, and application as structural probes. Biochemistry. 1983; 22(3):653–60. Epub 1983/02/01. https://doi.org/10.1021/bi00272a020 PMID: 6188482.

43. Hut HM, Lemstra W, Blaauw EH, Van Cappellen GW, Kampinga HH, Sibon OC. Centrosomes split in the presence of impaired DNA integrity during mitosis. Mol Biol Cell. 2003; 14(5):1993–2004. Epub 2003/06/13. https://doi.org/10.1091/mbc.e02-08-0510 PMID: 12802070; PubMed Central PMCID: PMC165092.

44. Wang J, Chang YF, Hamilton JI, Wilkinson MF. Nonsense-associated altered splicing: a frame-dependent response distinct from nonsense-mediated decay. Mol Cell. 2002; 10(4):951–7. Epub 2002/11/07. https://doi.org/10.1016/s1097-2765(02)00635-4 PMID: 12419238.

45. Sui T, Song Y, Liu Z, Chen M, Deng J, Xu Y, et al. CRISPR-induced exon skipping is dependent on premature termination codon mutations. Genome Biol. 2018; 19(1):164. Epub 2018/10/20. https://doi.org/10.1186/s13059-018-1532-z PMID: 30333044; PubMed Central PMCID: PMC6193291.

46. Littink KW, Pott JW, Collin RW, Kroes HY, Verheij JB, Blokland EA, et al. A novel nonsense mutation in CEP290 induces exon skipping and leads to a relatively mild retinal phenotype. Invest Ophthalmol Vis Sci. 2010; 51(7):3646–52. Epub 2010/02/05. https://doi.org/10.1167/iovs.09-5074 PMID: 20130272.

47. Roosing S, Cremers FPM, Riemslag FCC, Zonneveld-Vrieling MN, Talsma HE, Klessens-Godfroy FJM, et al. A Rare Form of Retinal Dystrophy Caused by Hypomorphic Nonsense Mutations in CEP290. Genes (Basel). 2017; 8(8). Epub 2017/08/23. https://doi.org/10.3390/genes8080208 PMID: 28829391; PubMed Central PMCID: PMC5575671.

48. Drivas TG, Wojno AP, Tucker BA, Stone EM, Bennett J. Basal exon skipping and genetic pleiotropy: A predictive model of disease pathogenesis. Sci Transl Med. 2015; 7(291):291ra97. Epub 2015/06/13. https://doi.org/10.1126/scitranslmed.aaa5370 PMID: 26062849; PubMed Central PMCID: PMC4486480.

49. Barny I, Perrault I, Michel C, Soussan M, Goudin N, Rio M, et al. Basal exon skipping and nonsense-associated altered splicing allows bypassing complete CEP290 loss-of-function in individuals with unusually mild retinal disease. Hum Mol Genet. 2018. Epub 2018/05/18. https://doi.org/10.1093/hmg/ddy179 PMID: 29771326.

50. Eley L, Gabrielides C, Adams M, Johnson CA, Hildebrandt F, Sayer JA. Jouberin localizes to collecting ducts and interacts with nephrocystin-1. Kidney Int. 2008; 74(9):1139–49. Epub 2008/07/18. https://doi.org/10.1038/ki.2008.377 PMID: 18633336.

51. Otto EA, Schermer B, Obara T, O'Toole JF, Hiller KS, Mueller AM, et al. Mutations in INVS encoding inversin cause nephronophthisis type 2, linking renal cystic disease to the function of primary cilia and left-right axis determination. Nat Genet. 2003; 34(4):413–20. Epub 2003/07/23. https://doi.org/10.1038/ng1217 PubMed Central PMCID: PMC3732175. PMID: 12872123

52. Mollet G, Salomon R, Gribouval O, Silbermann F, Bacq D, Landthaler G, et al. The gene mutated in juvenile nephronophthisis type 4 encodes a novel protein that interacts with nephrocystin. Nat Genet. 2002; 32(2):300–5. Epub 2002/09/24. https://doi.org/10.1038/ng996 PMID: 12244321.

53. Mollet G, Silbermann F, Delous M, Salomon R, Antignac C, Saunier S. Characterization of the nephrocystin/nephrocystin-4 complex and subcellular localization of nephrocystin-4 to primary cilia and centrosomes. Hum Mol Genet. 2005; 14(5):645–56. Epub 2005/01/22. https://doi.org/10.1093/hmg/ddi061 PMID: 15661758.

54. Hsu Y, Garrison JE, Kim G, Schmitz AR, Searby CC, Zhang Q, et al. BBSome function is required for both the morphogenesis and maintenance of the photoreceptor outer segment. PLoS Genet. 2017; 13 (10):e1007057. https://doi.org/10.1371/journal.pgen.1007057 PMID: 29049287; PubMed Central PMCID: PMC5663628.

55. Dilan TL, Singh RK, Saravanan T, Moye A, Goldberg AFX, Stoilov P, et al. Bardet-Biedl syndrome-8 (BBS8) protein is crucial for the development of outer segments in photoreceptor neurons. Hum Mol Genet. 2018; 27(2):283–94. Epub 2017/11/11. https://doi.org/10.1093/hmg/ddx399 PMID: 29126234; PubMed Central PMCID: PMC5886228.

56. Sedmak T, Wolfrum U. Intraflagellar transport proteins in ciliogenesis of photoreceptor cells. Biol Cell. 2011; 103(10):449–66. https://doi.org/10.1042/BC20110034 PMID: 21732910.

57. Caley DW, Johnson C, Liebelt RA. The postnatal development of the retina in the normal and rodless CBA mouse: a light and electron microscopic study. Am J Anat. 1972; 133(2):179–212. Epub 1972/02/01. https://doi.org/10.1002/aja.1001330205 PMID: 5009246.

58. Hildebrandt F, Zhou W. Nephronophthisis-associated ciliopathies. J Am Soc Nephrol. 2007; 18 (6):1855–71. Epub 2007/05/22. https://doi.org/10.1681/ASN.2006121344 PMID: 17513324.

59. Saunier S, Calado J, Benessy F, Silbermann F, Heilig R, Weissenbach J, et al. Characterization of the NPHP1 locus: mutational mechanism involved in deletions in familial juvenile nephronophthisis. Am J Hum Genet. 2000; 66(3):778–89. Epub 2000/03/11. https://doi.org/10.1086/302819 PMID: 10712196; PubMed Central PMCID: PMC1288163.

60. Coppieters F, Lefever S, Leroy BP, De Baere E. CEP290, a gene with many faces: mutation overview and presentation of CEP290base. Hum Mutat. 2010; 31(10):1097–108. https://doi.org/10.1002/humu.21337 PMID: 20690115.

61. Perrault I, Delphin N, Hanein S, Gerber S, Dufier JL, Roche O, et al. Spectrum of NPHP6/CEP290 mutations in Leber congenital amaurosis and delineation of the associated phenotype. Hum Mutat. 2007; 28(4):416. Epub 2007/03/09. https://doi.org/10.1002/humu.9485 PMID: 17345604.

62. Feldhaus B, Weisschuh N, Nasser F, den Hollander AI, Cremers FPM, Zrenner E, et al. CEP290 Mutation Spectrum and Delineation of the Associated Phenotype in a Large German Cohort: A Monocentric Study. American journal of ophthalmology. 2020; 211:142–50. Epub 2019/11/18. https://doi.org/10.1016/j.ajo.2019.11.012 PMID: 31734136.

63. Paloma E, Martinez-Mir A, Vilageliu L, Gonzalez-Duarte R, Balcells S. Spectrum of ABCA4 (ABCR) gene mutations in Spanish patients with autosomal recessive macular dystrophies. Hum Mutat. 2001; 17(6):504–10. Epub 2001/06/01. https://doi.org/10.1002/humu.1133 PMID: 11385708.

64. Apfelstedt-Sylla E, Theischen M, Ruther K, Wedemann H, Gal A, Zrenner E. Extensive intrafamilial and interfamilial phenotypic variation among patients with autosomal dominant retinal dystrophy and mutations in the human RDS/peripherin gene. Br J Ophthalmol. 1995; 79(1):28–34. Epub 1995/01/01. https://doi.org/10.1136/bjo.79.1.28 PMID: 7880786; PubMed Central PMCID: PMC505014.

65. Boon CJ, den Hollander AI, Hoyng CB, Cremers FP, Klevering BJ, Keunen JE. The spectrum of retinal dystrophies caused by mutations in the peripherin/RDS gene. Progress in retinal and eye research. 2008; 27(2):213–35. Epub 2008/03/11. https://doi.org/10.1016/j.preteyeres.2008.01.002 PMID: 18328765.

66. Del Pozo-Valero M, Martin-Merida I, Jimenez-Rolando B, Arteche A, Avila-Fernandez A, Blanco-Kelly F, et al. Expanded Phenotypic Spectrum of Retinopathies Associated with Autosomal Recessive and Dominant Mutations in PROM1. American journal of ophthalmology. 2019; 207:204–14. Epub 2019/05/28. https://doi.org/10.1016/j.ajo.2019.05.014 PMID: 31129250.

67. Mou H, Smith JL, Peng L, Yin H, Moore J, Zhang XO, et al. CRISPR/Cas9-mediated genome editing induces exon skipping by alternative splicing or exon deletion. Genome Biol. 2017; 18(1):108. Epub 2017/06/16. https://doi.org/10.1186/s13059-017-1237-8 PMID: 28615073; PubMed Central PMCID: PMC5470253.

68. Lalonde S, Stone OA, Lessard S, Lavertu A, Desjardins J, Beaudoin M, et al. Frameshift indels introduced by genome editing can lead to in-frame exon skipping. PLoS One. 2017; 12(6):e0178700. Epub 2017/06/02. https://doi.org/10.1371/journal.pone.0178700 PMID: 28570605; PubMed Central PMCID: PMC5453576.

69. Anderson JL, Mulligan TS, Shen MC, Wang H, Scahill CM, Tan FJ, et al. mRNA processing in mutant zebrafish lines generated by chemical and CRISPR-mediated mutagenesis produces unexpected transcripts that escape nonsense-mediated decay. PLoS Genet. 2017; 13(11):e1007105. Epub 2017/11/22. https://doi.org/10.1371/journal.pgen.1007105 PMID: 29161261; PubMed Central PMCID: PMC5716581.